Geological Quarterly, 2024, 68: 5
DOI: http://dx.doi.org/10.7306/gq.1728

Influence of Late Carboniferous–Early Permian climate change on the sedimentary evolution – a case study of the lacustrine Lower Anthracosia Shales (Intra-Sudetic Basin, SW Poland)

Jolanta DĄBEK-GŁOWACKA[1, 2, *], Patrycja WÓJCIK-TABOL[2] and Grzegorz J. NOWAK[3]

[1] Jagiellonian University, Doctoral School of Exact and Natural Sciences, Prof. St. Łojasiewicza 11, 30-348, Kraków, Poland; ORCID: 0000-0002-5158-9092

[2] Jagiellonian University, Institute of Geological Sciences, Gronostajowa 3a, 30-387 Kraków, Poland; ORCID: 0000-0001-5655-1619

[3] Polish Geological Institute – National Research Institute, Lower Silesian Branch, Jaworowa 19, 53-122 Wrocław, Poland; ORCID: 0000-0003-2228-5361

Dąbek-Głowacka, J., Wójcik-Tabol, P., Nowak, G.J., 2024. Influence of Late Carboniferous–Early Permian climate change on the sedimentary evolution – a case study of the lacustrine Lower Anthracosia Shales (Intra-Sudetic Basin, SW Poland). Geological Quarterly, 2024, 68: 5; https://doi.org/10.7306/gq.1728

Editor: Piotr Szrek

The Anthracosia Shales are lacustrine deposits within the volcano-sedimentary Pennsylvanian– Lower Permian succession of the Intra-Sudetic Basin. Core from the Rybnica Leśna PIG 1 borehole, which penetrated the Lower Anthracosia Shales, was analysed to explore the influence of climate on the evolution of the palaeolake, as distinct from tectonic and volcanic forcing. This reconstruction was made using mineralogical and geochemical proxies (elemental and mineralogical composition, TOC values, presence of framboidal pyrite and siderite). Based on the results, three chemically different intervals previously introduced by Wójcik-Tabol et al. (2021) are described. They represent the following stages of lake evolution: transgression (interval I), open lake (interval IIA and IIB), and termination (interval IIC and III). The initial stage of the lake (interval I) was probably related to a rise in humidity in the Late Pennsylvanian, linked to a southern Gondwana interglacial episode. Interval IIA represents the deepest facies of the Anthracosia Basin, where lake-floor anoxia prevailed. This stage was followed by a gradual lake-level fall recorded in interval IIB, with documented seasonality in humid and warm conditions. Interval IIC represents a stepwise lake regression attributed to aridification, as indicated by proxies showing a decrease in chemical weathering. Turbiditic sandy laminae in interval III reflect the terminal stage of lake infill.

Key words: lacustrine deposits, organic-rich deposits, palaeoclimate, geochemistry, Intra-Sudetic Basin.

INTRODUCTION

The Late Paleozoic is an example of the huge icehouse (Fielding et al., 2008) and records an important greenhouse gas-forced transition from a cold interval, including repeated phases of glaciation and deglaciation of the southern pole, to a fully greenhouse world (Montañez and Poulsen, 2013). Consequently, this time period is an excellent analogue for the present climate state (Gastaldo et al., 1996). Significant climatic transitions are shown in the Upper Carboniferous and Lower Permian rocks in different parts of Pangea. Palaeoclimatic reconstructions of the sedimentary succession from western tropical Pangea indicate the onset of seasonality in the Late Carboniferous and general aridification trend through the Early Permian. This trend was interrupted by several wet phases that might have been linked to the waxing and waning of the Gondwana icecap (Roscher and Schneider, 2006).

To study palaeoenvironmental changes, including palaeoclimate, lacustrine deposits are commonly sought-after, because lakes effectively accumulate sedimentary archives, with significant preservation potential in the geological record. Useful deep lacustrine lithofacies in this resepect are recognized in the Pennsylvanian and Lower Permian sequences of central Europe: in Poland (Dziedzic, 1959, 1961; Mastalerz, 1990; Mastalerz and Nehyba, 1997), the Czech Republic (Martínek et al., 2006; Lojka et al., 2009, 2010) and Germany (Uffmann et al., 2012).

We describe the petrological and geochemical record of the Pennsylvanian–Lower Permian of the Intra-Sudetic Basin, namely of the Lower Anthracosia Shales (LAS), in order to constrain the influence of climatic factors on the sedimentary sys-

* Corresponding author, e-mail: jolanta.dabek@doctoral.uj.edu.pl

Received: July 28, 2023; accepted November 20, 2023; first published online: April 4, 2024

tem, while also taking the contribution of tectonic and volcanic activity into consideration. The Anthracosia Shales have been previously described as regards their stratigraphic, palynological and sedimentological features, and their organic petrography (Dziedzic, 1959, 1961; Don, 1961; Miecznik, 1989; Lorenc, 1993; Bossowski and Ihnatowicz, 1994; Mastalerz and Nehyba, 1997; Nowak, 1998, 2003, 2007; Nowak et al., 2022; Kowalski and Furca, 2023).

This study explores the evolution of the Anthracosia Basin using integrated petrological and geochemical proxies: the size distribution of framboidal pyrite, elemental composition (Mo, Co, Mn enrichment; K/Ti, Ca/Ti, Zr/K ratios; and elemental trends of P, Al, Si, Ti and Zr), mineralogical composition (siderite, calcite) and TOC values. Based on the results, a tripartite division previously established in the LAS in the Rybnica Leśna PIG 1 based on lithology (Wójcik-Tabol et al., 2021) is detailed and used to document different stages of lake evolution.

GEOLOGICAL SETTING

The Intra-Sudetic Basin forms the easternmost part of the intramontane basin system of the Bohemian Massif. The basin formed in the Early Carboniferous as an internal molasse basin during the Varicides development. The Intra-Sudetic Basin constitutes a large fault-bounded structure, 70 km long and 35 km wide, which extends WNW–ESE (Nemec et al., 1982; Dziedzic and Teisseyre, 1990; Bossowski and Ihnatowicz, 1994, 2006; Awdankiewicz et al., 2003; Mazur et al., 2006; Fig. 1).

The history of the Intra-Sudetic Basin started in the Early Carboniferous, when the basin accumulated non-marine, clastic deposits: mostly coarse-grained conglomerates and breccias. A Late Visean transgression established marine conditions in the basin while at the end of Visean, tectonic uplift led to marine regression, initiating sedimentation in continental conditions which lasted to the end of the Autunian age. The Upper Carboniferous–Lower Permian succession is characterized by a few individual fining-upwards megacyclothems (Awdankiewicz et al., 2003). Marine and continental basinal deposits are intercalated with volcaniclastic material, a residue of volcanic activity that took place in the latest Tournaisian/earliest Visean, the Middle and Late Pennsylvanian, and the Early Permian (Awdankiewicz, 1999; Awdankiewicz et al., 2003).

Lacustrine in origin, the Anthracosia Shales constitute the uppermost parts of two megacyclothems, these being: the Lower Anthracosia Shales that belongs to the Ludwikowice Formation and the Upper Anthracosia Shales (UAS) within the Krajanów Formation (Fig. 1; Bossowski and Ihnatowicz, 1994). The LAS are part of the first generally barren succession following deposition of coal-bearing strata. This sedimentary succession starts with reddish sandstones and conglomerates characteristic of alluvial-fluvial settings. The uppermost part of this formation consists mostly of fine-grained dark grey lacustrine deposits. Within these, two lithofacies of the Anthracosia Shales can be distinguished: grey and greenish to dark brown micaceous mudstones and sandstones intercalated with thin limestones; and bituminous dark shales intercalated with thin coal layers (Dziedzic, 1959).

The term “Anthracosia” is related to the late Carboniferous non-marine bivalve *Anthraconaia* (Eagar, 1987). Although these fossils are not found in all sections of the LAS and UAS, they are the basis for a regional term used for several decades.

The exact age of both Anthracosia Shale units remains unknown. Firstly, the boundary between Pennsylvanian and Autunian deposits was placed arbitrarily by German geologists in the beginning of 20th century, mostly by the dominant rock colour: deposits with a reddish colouration were assigned to the Autonian (Dziedzic, 1971). Using this assumption, the LAS and UAS

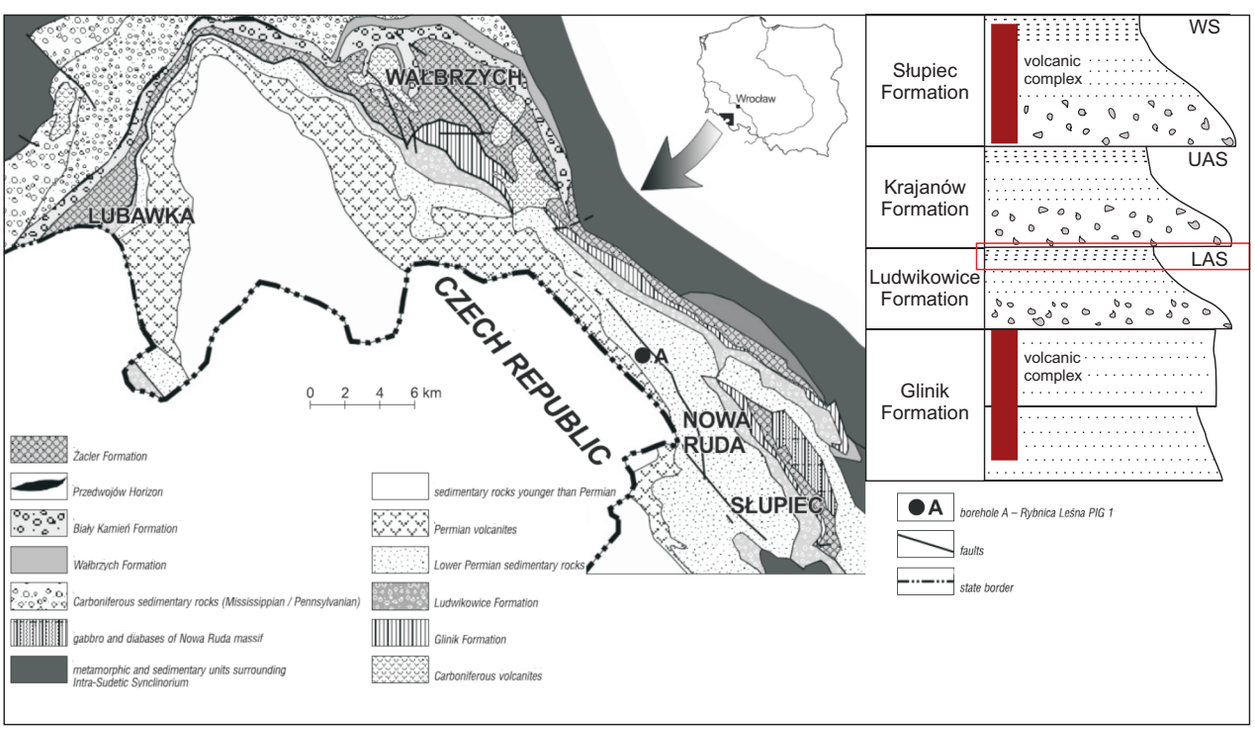

Fig. 1. Generalized geological map of the Intra-Sudetic Basin (according to Bossowski and Ihnatowicz, 2006; simplified) with lithostratigraphic position of the Anthracosia Shales

WS – Walchia Shales, UAS – Upper Anthracosia Shales, LAS – Lower Anthracosia Shales

are Autunian. Later, their age was constrained by palynological studies by two research teams: one indicated a latest Pennsylvanian (Stephanian age) (Górecka, 1981; Górecka-Nowak, 1989, 1995, 2008; Trzepierczyńska, 1994; Górecka-Nowak and Nowak, 2008), the other suggesting the Autunian (to earliest Cisuralian; Jerzykiewicz, 1987). In this study, the LAS is considered as Pennsylvanian/Autunian.

MATERIAL AND METHODS

Samples were collected from the LAS drilled in the Rybnica Leśna PIG 1 borehole situated in the NE part of the Intra-Sudetic Basin (Fig. 1). The borehole reached a depth of 200 m, the LAS comprising a 61.5 m thick interval ranging from 95.0 to 156.5 m. Twenty four samples were taken from the LAS (Fig. 2) interval.

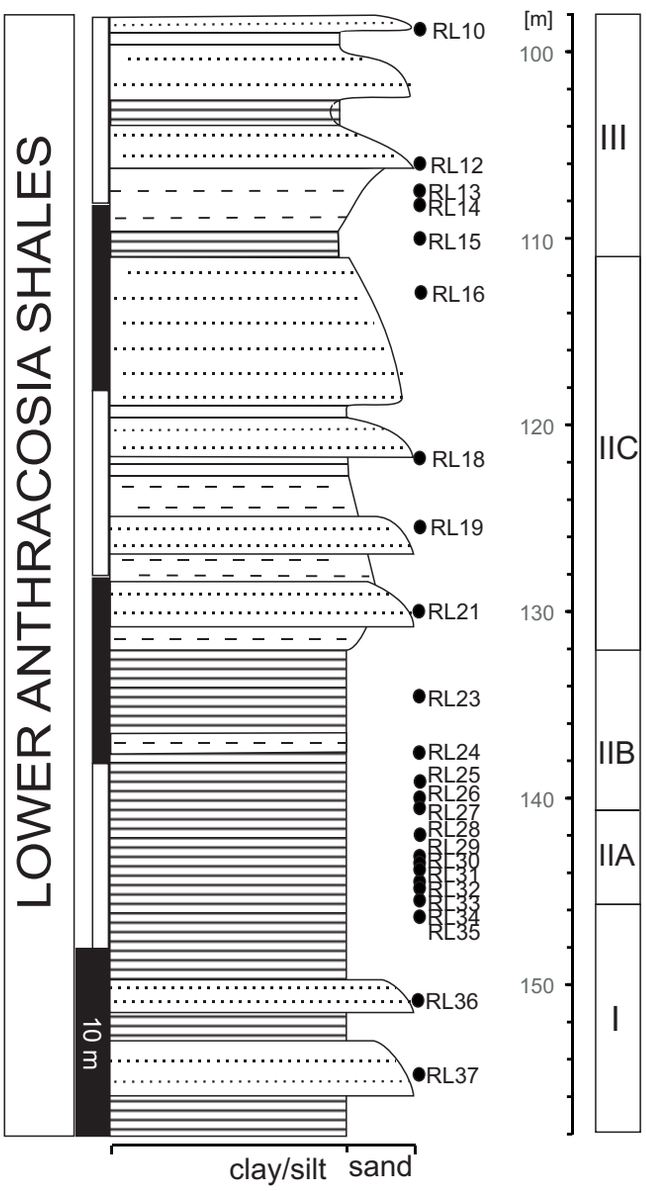

Fig. 2. Lithological log of the Lower Anthracosia Shales in the Rybnica Leśna PIG 1 borehole with sampling locations and distinguished rock intervals marked

METHODS

X-ray diffraction (XRD) quantitative analysis of 7 LAS samples (Table 1) was performed to characterize the mineral composition. To pre-crushed samples, 10% of ZnO were added, then they were ground in a McCrone mill and slides made in sideloaded cuvettes. They were analysed using a *Philips X'Pert APD* diffractometer, equipped with a *PW3020* vertical goniometer and a graphite monochromator. CuKα radiation was applied with an accelerating voltage of 40 kV and a cathode heating current of 30 mA. Measurement was made in the angle range of 2–65° 2 with a speed of 0.02°/5s. Diffractograms were analysed with the use of the *ClayLab* and *AutoQuan* programs. *Profex* software (Döbelin and Kleeberg, 2015) was used to determine quantitative mineral composition.

To analyse the characteristics of the pyrite, thin-sections from 5 samples (Table 1) from intervals IIA and IIB were observed by optical microscopy in reflected light at a magnification of 1000 ×. A *Nikon Eclipse E600-POL* polarizing microscope was used, and the pyrite photos were recorded using a *Canon EOS 400* digital camera controlled by the *Canon EOS Utility* program. All forms of pyrite present were photographed and then, using the *JMicroVision* program, the diameters of 100 framboids for each sample were measured. The minimum/maximum, mean and standard deviation of the framboids' diameters were documented. After optical microscope observation, the same 5 thin-sections were coated with carbon and photographed using a *HITACHI S-4700* microscope with a *NORAN Vantage* microanalysis system. Observation was made with the *YAGBSE* detector to obtain framboidal pyrite photos.

Table 1

Samples numbers with performed analyses

Sample	XRD-quantitative analysis	Thin-sections observations	SEM observations	ICP-OES
RL10				x
RL12	x			x
RL13				x
RL14				x
RL15	x			
RL16				x
RL18				x
RL19				x
RL21	x			x
RL23				x
RL24		x	x	x
RL25	x			x
RL26		x	x	x
RL27		x	x	x
RL28	x			
RL29				x
RL30	x	x	x	
RL31				x
RL32				x
RL33		x	x	
RL34				x
RL35				x
RL36				x
RL37	x			x

Seventeen samples (Table 1) were selected for elemental composition analysis with the use of inductively coupled plasma-optical emission spectrometry (*ICP-OES*) Additionally, 3 siderite samples were prepared from laminae of yellowish siderite. Powdered samples were mineralized in a mixture of spectrally clean, concentrated nitric, hydrochloric and hydrofluoric acids. Elemental analyses were carried out using an *ICP-OES Spectro Arcos* spectrometer (SPECTRO Analytical Instruments GmbH, Kleve, Germany) with the radial (side-on) viewed torch configuration to measure the major elements and with axial (end-on) torch configuration to measure trace elements. Certified reference material *OREAS 920 Certified* reference material *OREAS 920* (Oreas®, Melbourne, Australia) was processed and measured every 10 samples in the same manner as the samples in the same analytical cycle to monitor the accuracy of the analyses. Values obtained for the latter between 95 and 105% of the certified values were accepted.

To estimate the trace metal enrichment in the samples, the Al-normalized enrichment factor was used and normalized to the average shale (Li and Schoonmaker, 2003). The values were obtained using the following equation:

$$EF\ X = [(X/Al)\ sample/(X/Al)\ average\ shale]$$

where: X and Al represent the content of element X and aluminum, respectively.

The Pearson coefficient (r) was utilized to express the relationships between the chemical components. The Pearson correlation values were calculated using *TIBCO Statistica* software.

RESULTS

Based on the geochemical results obtained, the three rock intervals identified by Wójcik-Tabol et al. (2021) were described in detail, with the addition of subintervals. They are as follows (Fig. 2):

- Interval I (from 145.5 to 156.5 m) is developed as pale grey medium- and fine-grained laminated sandstones intercalated with thin layers of mudstone and unfossiliferous shale (Fig. 3A); the laminations here are emphasized by changes in grain size;
- Interval II (from 111 to 145.5 m) is further subdivided into subintervals IIA–IIC, according to their mineralogical and geochemical features;
- Interval IIA (5 m thick) consists of massive calcareous dark grey shales lacking, or with very subtle, horizontal lamination (Fig. 3B). This interval is characterized by poorly developed rhythmic changes in the organic-rich clayey matrix. A single *Anthraconaia* bivalve impression was recognized in one of the samples (Fig. 3C);
- Interval IIB (8 m thick) consists of dark organic-rich shales with thin sandstone and siderite intercalations. Siderite is present here in the form of layers and lenses with a maximum thickness of 1 cm (Fig. 3D). In contrast to the shales from interval IIA, interval IIB is characterized by well-defined lamination;
- Interval IIC (21.5 m thick) is composed of shales with a greater number of fine-grained sandstone intercalations and the presence of siderite concretions (Fig. 3E). Visible

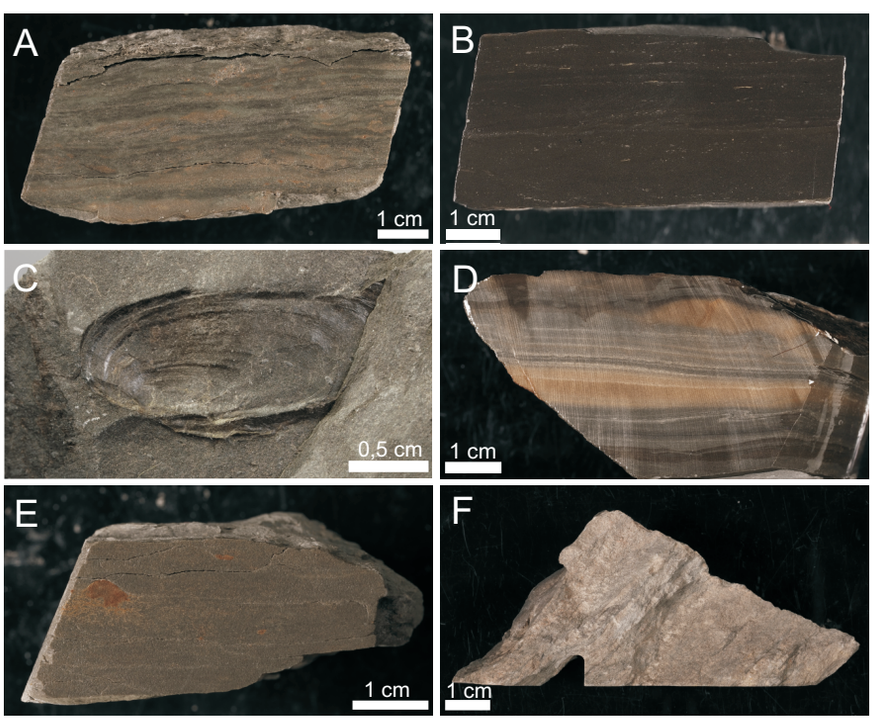

Fig. 3A – grey laminated sandstone (lighter layers) with mudstone intercalations (darker layers) from interval I; B – dark claystone with slightly visible horizontal lamination from interval IIA; C – dark claystone with *Anthraconaia* bivalve print from interval IIA; D – laminated claystone with layers of yellowish siderite from interval IIB; E – grey fine-grained sandstone with siderite concretions from interval IIC; F – light grey fine-grained sandstone from interval III

lamination is emphasized by changes in grain size and the distribution of organic matter;

– Interval III (from 98 to 111 m) is composed of fine to medium-grained sandstones with thin shale layers (Fig. 3F).

MINERAL COMPOSITION

The mineral composition of the samples analysed is shown on Figure 4. All samples have essentially the same composition, comprising quartz, feldspar, micas (muscovite) and clay minerals (illite, kaolinite and chlorite). The samples differ from each other in the presence of carbonates (siderite and calcite) and pyrite. In the composition of interval IIA, pyrite and calcite appears. In interval IIB, calcite is replaced by the siderite, which forms lenses ~0.5 cm thick. In intervals IIC and III there is a small amount of siderite in the form of concretions.

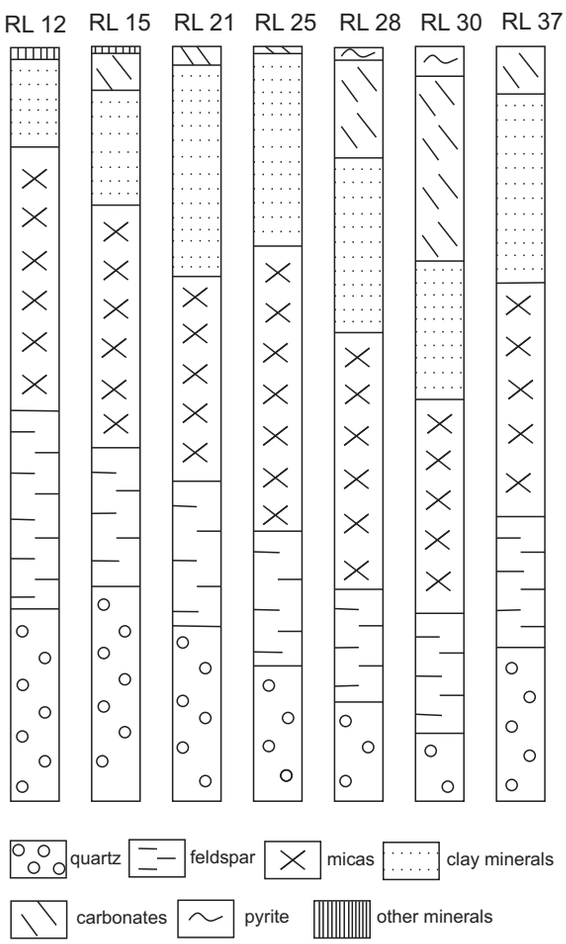

Fig. 4. Mineral composition of selected samples from the LAS

FRAMBOID SIZE ANALYSIS

All pyrite detected pyrite was within intervals IIA and IIB, in dark grey claystone. It occurs both within and outside the siderite layers. The forms of pyrite were detected comprised framboids (Fig. 5), ie. spherical aggregates of pyrite grains resembling raspberries (Rust, 1935), euhedral crystals, and replacements of organic matter. Euhedral crystals are the most abundant form of pyrite found in all the samples analysed. They strongly vary in size, from <0.5 up to 17 m. They occur in a clustered form more frequently than as single crystals, in contrast to the framboids, which usually occur separately, locally in the company of euhedral crystals and least often in clusters. The framboids are built with microcrystals that are generally not larger than 1 m, though their sizes can vary slightly within a single framboid, and they can be packed densely or loosely. Microcrystals that build framboids are generally well-formed (Fig. 5A–E, H–I), though some of them have holes inside (Fig. 5F, G). Besides perfectly spherical shapes (Fig. 5C, I), they also tend to occur as ellipsoidal (Fig. 5E, H) and irregular framboids (Fig. 5D).

The characteristics of the framboid size among the samples and frequency of framboid diameters are given in Table 2 and Figure 6.

According to the classification of redox conditions based on framboid size distribution (Bond and Wignall, 2010; Liu et al., 2021), we can distinguish 4 ranges:

1 – abundant framboids up to 6 m in diameter, which can indicate anoxic bottom water;

2 – framboids with a mean size of 6–10 m that can indicate dysoxic bottom water;

3 – framboids with a mean size of 10–20 m, which can indicate dysoxic-to-oxic conditions;

4 – a lack of framboids, that can characterize oxic bottom waters.

The largest group of framboids in the LAS represents that with a diameter up to 6 m. Framboids with a diameter ranging between 6 and 10 m form the second-most-numerous group, and the largest framboids, of diameter >10 m, make up the smallest percentage of the framboids measured. The contribution of framboidal pyrite up to 6 m varies from 72% in the lower part of the pyrite occurrence interval (interval IIA) to 39% at its upper part (interval IIB) (Fig. 5). The distribution of the sizes shows that in interval IIA we have generally smaller framboids and their size slightly increases on going upwards to interval IIB.

MAJOR AND TRACE ELEMENTS AND TOC VALUES

The chemical composition of the samples studied is shown in Table 3.

Aluminum, potassium and silicon have an affinity for phyllosilicates and quartz. The Zr content is related to detrital heavy minerals. Ti can be combined with both heavy minerals and phyllosilicates. The elements of the siliciclastic group (Al, Si, K, Ti, Zr) are positively correlated with each other (Table 4). Their content displays a slight fall in the calcareous interval IIA before increasing towards the top of the section (Fig. 7). The relative change in K is expressed by the K/Ti and Zr/K ratios that fluctuate from 5.3 to 9 and from 0.023 to 0.049, respectively (Table 3). The profiles of the K/Ti and Zr/K ratios show a K minimum in the sideritic black claystones (interval IIB). The relative content of K rises gradually upwards in the section towards interval III. A positive excursion in Zr content occurs in the upper part of the section (Fig. 7).

These lithogenic elements reveal strong negative correlation with Fe, Ca and Mn (Table 4), indicating that the latter are mostly situated in the carbonate phase (calcite and siderite). Elevated Ca/Ti ratios in interval IIA (Table 3) indicate a minimum of siliciclastic sedimentation in interval IIA. The Ca/Ti ratios are moderately high in the sideritic interval IIB, while in the rest of the intervals Ca/Ti is rather low (Fig. 7).

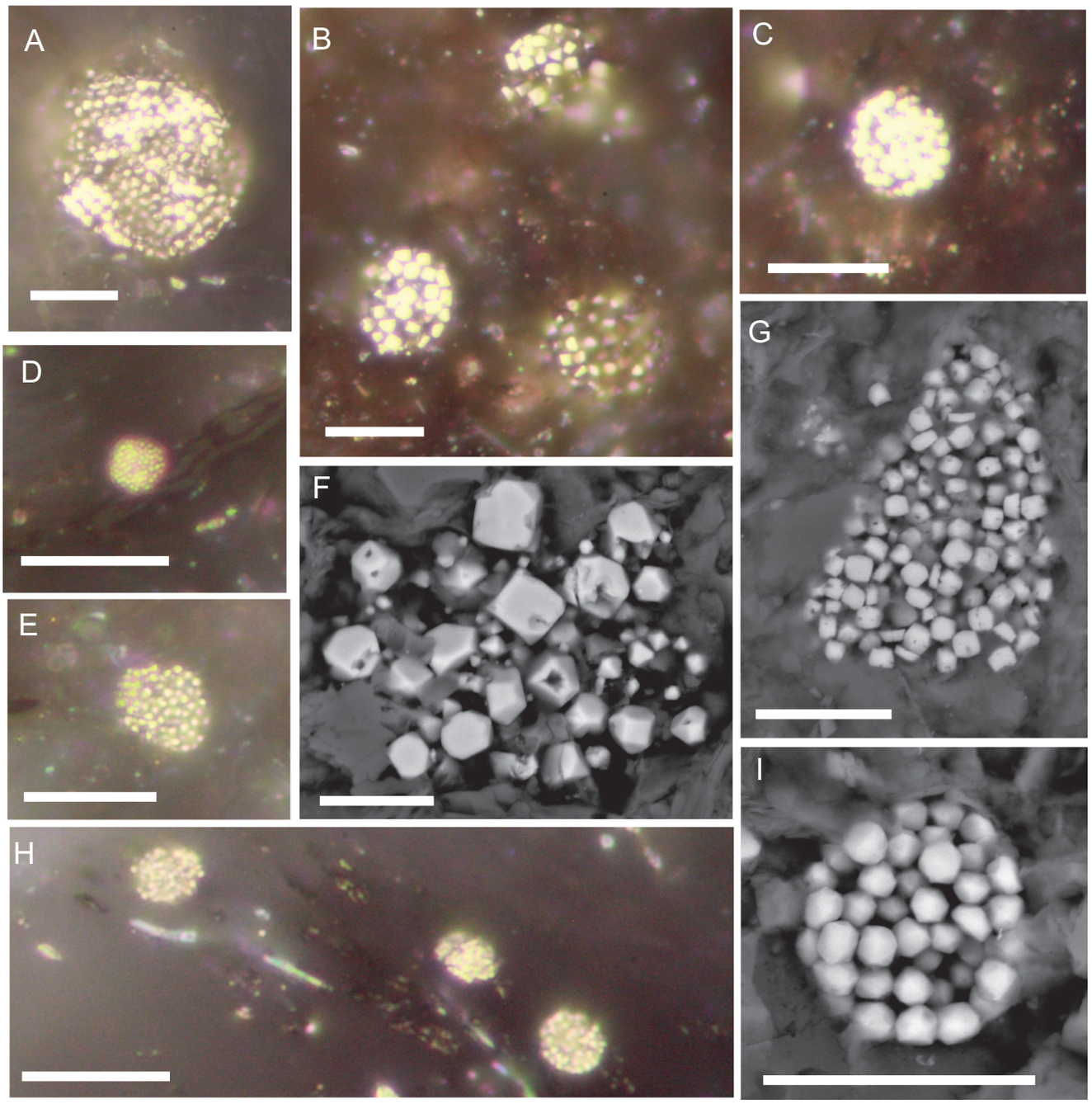

Fig. 5. Morphologies of pyrite that occur in the LAS

A – round framboid from RL26; **B** – group of 3 round framboids from RL30; **C** – round framboid from RL30; **D** – small framboid with irregular shape from RL26; E – framboid with irregular shape from RL24; **F** – cluster of pyrite crystals that differ in size from RL27, where larger crystals are characterized with pores in their central parts; **G** – cluster of pyrite crystals that are approximately the same in size from RL30, with crystals also characterized by pores in their central parts; **H** – 3 ellipsoidal framboids from RL26; **I** – round framboid from RL37; photos from reflected light (A–E, G) and scanning electron microscope (SEM) with YAGSBE detector (F, H, I); scale bar: 10 m

The Fe content is moderately high and strongly fluctuating in interval IIB. These values reflect sideritic interlayers. The Fe content drops in interval IIC, and then decreases stepwise upwards in the section. The content of Mn reveals maximum excursions in the sideritic layers that show the highest Mn/Fe ratios. The sideritic layers are also enriched in P and Co. Calcareous claystones in Interval IIA show the highest contents of Ca and TOC. An enrichment in P, S and Mo (Fig. 7) was also noted here.

INTERPRETATION

TERRIGENOUS INPUT AND CLIMATE CHANGE

Elements such as Al, Si, Ti and Zr are commonly used as a proxy of detrital input (Taylor and McLennan, 1985; Rachold and Brumsack, 2001). As weathering and/or diagenetic pro-

Table 2

Size characteristics of framboids from the LAS

Sample	n	Min diameter [m]	Max diameter [m]	Mean [m]	Standard deviation [m]
RL24	100	2.62	16.49	7.58	3.42
RL26	100	1.86	42.08	7.32	5.42
RL27	100	1.99	22.59	5.79	3.18
RL30	100	1.67	21.19	6.96	3.29
RL33	100	1.82	13.97	5.25	2.42

cesses barely affect their concentration (Calvert and Pedersen, 1993), they can be used as a reliable indicator of terrigenous flux in the LAS. Additionally, mineralogical data can also be useful here and support the geochemical data.

X-ray diffraction results of the LAS (Fig. 4) reveal that the calcareous claystones of interval IIA contain the lowest amounts of siliciclastics (clay minerals and quartz) and the appearance of calcite. The mineral composition is mirrored in chemical features such as the low content of lithogenic elements (Al, Si, K, Ti, Zr) and high Ca/Ti ratio (Fig. 7). Upwards in the section, the terrestrial input increases, as expressed by elevated contents of Al, Si, K, Ti and Zr. Elevated Zr values in the upper part of the section may also indicate some contribution of felsic volcanoclastic rocks.

Climate is one of the factors that may be responsible for the intensity of chemical weathering in the source region. This might be established by comparison of the content of water-soluble (e.g., K) and less mobile (e.g., Al and Ti) elements, which are differentiated during mineral decay in a warm and humid environment. The palaeoclimatic indices used are as follows: the K/Ti ratio, showing the degree of chemical alteration; the Ca/Ti ratio, reflecting changes in detrital input; and the Zr/K ratio, being a measure of inflow energy (Dypvik and Harris, 2001; Arnaud et al., 2012; Bassetti et al., 2016).

The general distribution of the Zr/K ratio (Fig. 7) suggests an increase in transport energy upwards in the LAS section. Some fluctuation of the Zr/K ratio is revealed, and this may correspond to variations in of Zr contents, which might reflect changing grain size in the terrigenous fraction. Zr carrier minerals are usually associated with generally turbulent silt-sand sedimentation, and thus the Zr enrichment in the deposits may be related to more humid conditions (with intense precipitation and fluvial

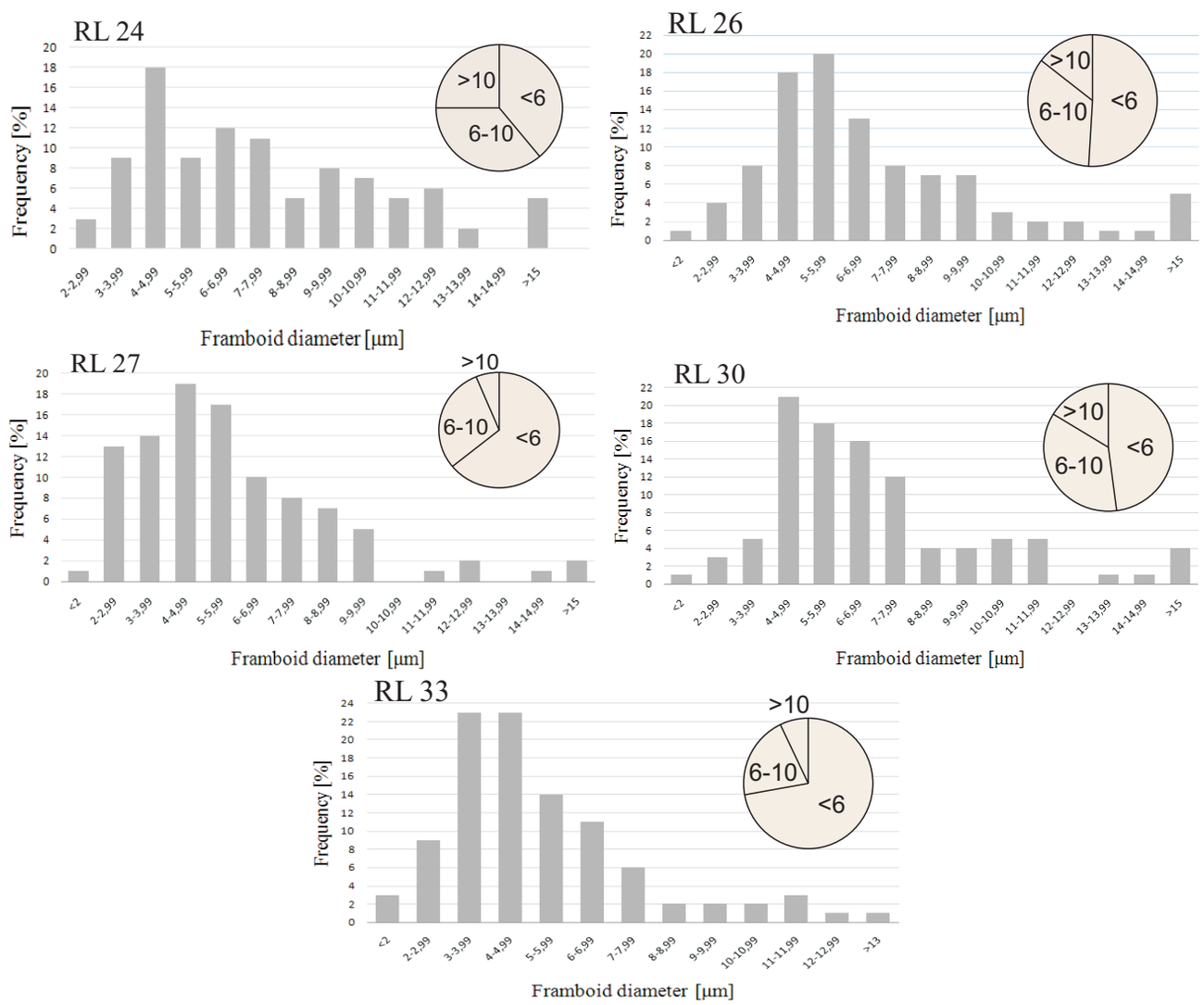

Fig. 6. Graphs with frequencies of framboid diameters

Table 3

Chemical composition of samples of the Lower Anthracosia Shales from the Rybnica Leśna PIG 1 borehole core section

			Sample	TOC	Al	Ca	Fe	K	Mn	P	TS	Si	Ti	Zr	Mo	Co	K/Ti	K/Al	Ca/Ti	Zr/K	Zr/Al	Mn/Fe
Interval	Lithology	Depth		wt.%	%				ppm	%				ppm								
III	greenish fin-egrained sandstone	99.5	RL10	nd	15.87	0.22	1.82	6.12	68	0.06	0.02	23.30	0.91	236	1.59	10	6.75	0.39	0.25	0.039	0.015	0.004
	grey fine-grained sandstone	105.9	RL12	0.26	10.67	0.31	2.35	4.21	514	0.07	0.04	26.80	0.67	207	1.54	12	6.30	0.39	0.47	0.049	0.019	0.022
	grey mudstone	108.3	RL13	0.8	12.47	0.59	3.82	5.55	612	0.08	0.04	23.10	0.62	145	1.34	17	8.97	0.44	0.95	0.026	0.012	0.016
	grey mudstone	108.35	RL14	1.07*	14.37	0.37	2.25	5.76	178	0.08	0.08	24.70	0.68	151	1.69	13	8.45	0.40	0.54	0.026	0.011	0.008
IIC	grey fine-grained sandstone	113.2	RL16	0.48*	14.37	0.24	3.50	5.92	376	0.05	0.08	23.90	0.67	145	1.56	19	8.90	0.41	0.36	0.024	0.010	0.011
	grey fine-grained sandstone	121.9	RL18	0.2	13.17	0.28	2.00	5.06	148	0.05	0.02	27.40	0.70	182	1.50	8	7.19	0.38	0.40	0.036	0.014	0.007
	grey fine-grained sandstone with siderite concretions	125.5	RL19	0.24	12.27	0.36	3.12	4.76	594	0.05	0.03	25.80	0.65	153	0.99	14	7.35	0.39	0.56	0.032	0.012	0.019
	grey fine-grained sandstone	129.5	RL21	1.04	10.97	0.37	3.49	3.65	498	0.08	0.09	26.20	0.63	162	2.94	19	5.84	0.33	0.59	0.044	0.015	0.014
IIB	grey mudstone	134.6	RL23	1.1*	13.47	0.31	3.70	4.38	325	0.07	0.07	25.10	0.68	158	2.07	25	6.40	0.33	0.45	0.036	0.012	0.009
	grey claystone with siderite laminations	137.7	RL24	0.99*	13.17	0.38	4.93	4.09	638	0.08	0.18	25.70	0.65	148	1.18	24	6.27	0.31	0.58	0.036	0.011	0.013
			RL24 SYD		8.35	0.91	16.80	2.68	4122	0.09	0.25	18.90	0.45	97	0.05	19	5.93	0.32	2.01	0.036	0.012	0.025
	grey claystone with siderite laminations	138.7	RL25	0.89	13.87	0.33	4.19	4.08	466	0.07	0.06	25.10	0.65	146	1.96	26	6.24	0.29	0.51	0.036	0.011	0.011
			RL25 SYD		10.07	0.63	11.30	3.08	3469	0.10	0.17	21.10	0.49	110	0.05	23	6.30	0.31	1.28	0.036	0.011	0.031
	grey claystone with siderite laminations	140.25	RL26	1*	12.97	0.30	4.02	3.92	441	0.07	0.08	26.20	0.71	168	1.66	22	5.55	0.30	0.42	0.043	0.013	0.011
	grey claystone with siderite laminations	140.3	RL27	0.91	11.57	0.57	7.42	3.70	1456	0.10	0.13	24.00	0.60	134	0.85	21	6.17	0.32	0.95	0.036	0.012	0.020
			RL27 SYD		7.48	1.26	15.40	2.37	3520	0.09	0.07	20.00	0.45	95	0.05	11	5.33	0.32	2.83	0.040	0.013	0.023
IIA	dark grey claystone	142.85	RL 29	0.52*	10.97	5.60	5.28	3.50	788	0.09	2.24	20.00	0.52	114	2.35	21	6.80	0.32	10.87	0.033	0.010	0.015
	dark grey claystone	143.9	RL31	2.13*	7.66	19.00	3.79	2.67	953	0.12	1.93	14.40	0.37	86	3.41	13	7.30	0.35	51.91	0.032	0.011	0.025
	dark grey claystone	144.2	RL32	2.25*	10.37	7.54	4.61	3.64	923	0.14	2.10	19.60	0.48	108	9.42	17	7.66	0.35	15.87	0.030	0.011	0.020
	dark grey claystone	145.5	RL34	1.46	12.07	4.86	4.06	3.81	735	0.08	1.78	20.40	0.47	100	62.80	17	8.11	0.32	10.34	0.026	0.008	0.018
I	grey claystone	146.7	RL35	0.29	15.37	0.96	3.41	4.58	228	0.10	0.04	24.80	0.56	165	1.72	10	8.15	0.30	1.71	0.036	0.011	0.007
	grey fine-grained sandstone	150.6	RL36	0.21*	13.57	0.63	4.64	4.23	395	0.08	0.04	25.10	0.70	159	1.97	20	6.06	0.31	0.91	0.038	0.012	0.009
	grey fine-grained sandstone	154.8	RL37	0.05*	16.67	0.49	4.32	4.79	337	0.05	0.53	23.60	0.56	109	3.50	30	8.58	0.29	0.88	0.023	0.007	0.008

* – analysed and described by Nowak et al. (2022)

Table 4

Pearson correlation matrix for selected elements in samples (p <0.05, n = 23)

	Al	K	Ti	Si	Zr	Co	Mo	S	Ca	P	Fe	Mn
Al	1.00	0.82	0.70	0.62	0.55	0.19	–0.01	–0.36	–0.49	–0.56	–0.63	–0.71
K	0.82	1.00	0.76	0.56	0.66	–0.15	–0.08	–0.38	–0.43	–0.56	–0.68	–0.69
Ti	0.70	0.76	1.00	0.77	0.91	–0.08	–0.27	–0.60	–0.61	–0.62	–0.56	–0.59
Si	0.62	0.56	0.77	1.00	0.75	0.05	–0.23	–0.71	–0.78	–0.64	–0.47	–0.52
Zr	0.55	0.66	0.91	0.75	1.00	–0.33	–0.27	–0.57	–0.51	–0.48	–0.58	–0.57
Co	0.19	–0.15	–0.08	0.05	–0.33	1.00	–0.02	0.03	–0.16	–0.14	0.12	0.04
Mo	–0.01	–0.08	–0.27	–0.23	–0.27	–0.02	1.00	0.47	0.21	0.06	–0.11	–0.09
S	–0.36	–0.38	–0.60	–0.71	–0.57	0.03	0.47	1.00	0.79	0.55	–0.05	0.00
Ca	–0.49	–0.43	–0.61	–0.78	–0.51	–0.16	0.21	0.79	1.00	0.62	–0.05	0.02
P	–0.56	–0.56	–0.62	–0.64	–0.48	–0.14	0.06	0.55	0.62	1.00	0.28	0.34
Fe	–0.63	–0.68	–0.56	–0.47	–0.58	0.12	–0.11	–0.05	–0.05	0.28	1.00	0.97
Mn	–0.71	–0.69	–0.59	–0.52	–0.57	0.04	–0.09	0.00	0.02	0.34	0.97	1.00

transportation) (Dypvik and Harris, 2001). In this interpretation, intervals IIB and III were influenced by more humid conditions. If falling Zr content suggests a reduction of sedimentary transport (Bassetti et al., 2016; Grabowski et al., 2021a), the transition from interval IIC to interval III would represent a more arid environment. By comparison, interval IIA is overall poor in far-travelled components due to the hemipelagic open-lake deposition it represents. The K/Ti ratio can be additionally used as an indirect palaeoclimate proxy (Arnaud et al., 2012; Clift et al., 2014; Grabowski et al., 2021b), indicating an increase in chemical alteration towards interval IIB.

Another palaeoclimate clue in the lacustrine facies is siderite occurrence. Siderite is an autochthonous component of modern and ancient tropical lakes that precipitates by synsedimentary or very early diagenetic reduction of ferric (oxyhydr)oxides, originating from terrestrial weathering favoured by a humid and warm climate (Irion et al., 2006; Lojka et al., 2009). Siderite occurring in particular laminae can indicate the limitation of its crystallization to certain periods when favourable conditions prevailed, and this may have been be related to seasonality at the lake bottom (Bahrig, 1989). Siderite occurrence in the LAS is reflected in the Fe content. It is inferred that the highest Fe accumulation in interval IIB records the weathering maximum, before this weakened, and Fe levels fell in interval IIC.

The mineralogical and geochemical data obtained from the LAS indicate that changes in terrigenous influx might be attributed to global climatic factors, while tectonic uplift and volcanic activity cannot be excluded.

REDOX CONDITIONS

Redox analysis is a standard feature of palaeoenvironmental studies, and various sedimentary geochemical proxies have been developed. Besides the macroscopic features such as visible lamination and grey-black colours caused by OM accumulation, the presence of pyrite, especially framboidal pyrite, can be used as an indicator of redox conditions. The formation of pyrite requires the presence and availability of iron and sulphur in the sedimentary basin; therefore, organic-rich sediments are usually environments encouraging pyrite growth (Sawłowicz, 1993, 2000). Pyrite can be found in sedimentary rocks in the form of individual euhedral crystals, spherical framboids built with microcrystals, and substituting organic matter.

Besides the presence of pyrite, framboid morphology and size characteristics can also be useful to infer environmental conditions in the basin (Wilkin et al., 1996; Bond and Wignall, 2010). The lack of sediment within framboid voids from the LAS suggests that they are not diagenetic in origin and so can be used as a redox proxy (Wei and Jiang, 2019). The hollow microcrystals shown on Figure 5F and H can indicate rapid growth in a highly supersaturated environment (Berg, 1938). Regarding the framboid shape, ellipsoidal forms (Fig. 5C, D) may be a result of deformation of primarily spheroidal framboids (Rickard, 2021).

It has been commonly observed that pyrite framboids found in recent anoxic environments are on average smaller and less variable in size than those framboids collected from sediments underlying oxic or dysoxic water columns. It has also been suggested that syngenetic framboid size does not significantly increase with time post-deposition (Wilkin et al., 1996); therefore, the size distribution of framboidal pyrite in sedimentary rocks might be recognized as a redox indicator (Wilkin et al., 1996; Yuan et al., 2017). Framboid size distribution in the LAS suggests anoxic-dysoxic conditions in the water mass during pyrite formation (black claystones of interval IIA and IIB). Additionally, changes in framboid size – especially framboids up to 6 m and bigger than 10 m – show the transition from the more anoxic conditions in interval IIA to dysoxic conditions in interval IIB (Fig. 6). Intervals I, IIC and III are barren of pyrite, which may indicate more oxygenated conditions during their formation (Liu et al., 2021).

Another indicator of redox conditions used in this paper is an accumulation of some trace elements (e.g., Mo, Co, Mn, Fe) that are redox-sensitive (e.g., Algeo and Maynard, 2004; Liu et al., 2021). The LAS are rather poor in trace elements in comparison with average shale (Li and Schoonmaker, 2003). However, the black claystones of interval IIA are enriched in Mo (Fig. 7), suggesting anoxic conditions. Molybdenum is here accompanied by TS and TOC. This is an obvious association because the transfer of MoO_4^{2-} to the sediment is likely promoted through adsorption onto organic or mineral particles. In anoxic sediments, Mo (VI) is reduced to Mo (V) (e.g., MoO^{2+}) or Mo (IV) species (e.g., thiomolybdate) (Calvert and Pedersen, 1993). They can be deposited as organic thiomolybdates or, after further reduction, in solid solution with Fe-sulphides (Helz et al., 1996; Tribovillard et al., 2006). Mo displays little affinity to a $CaCO_3$ surface, but Mo immobilization requires a reduction

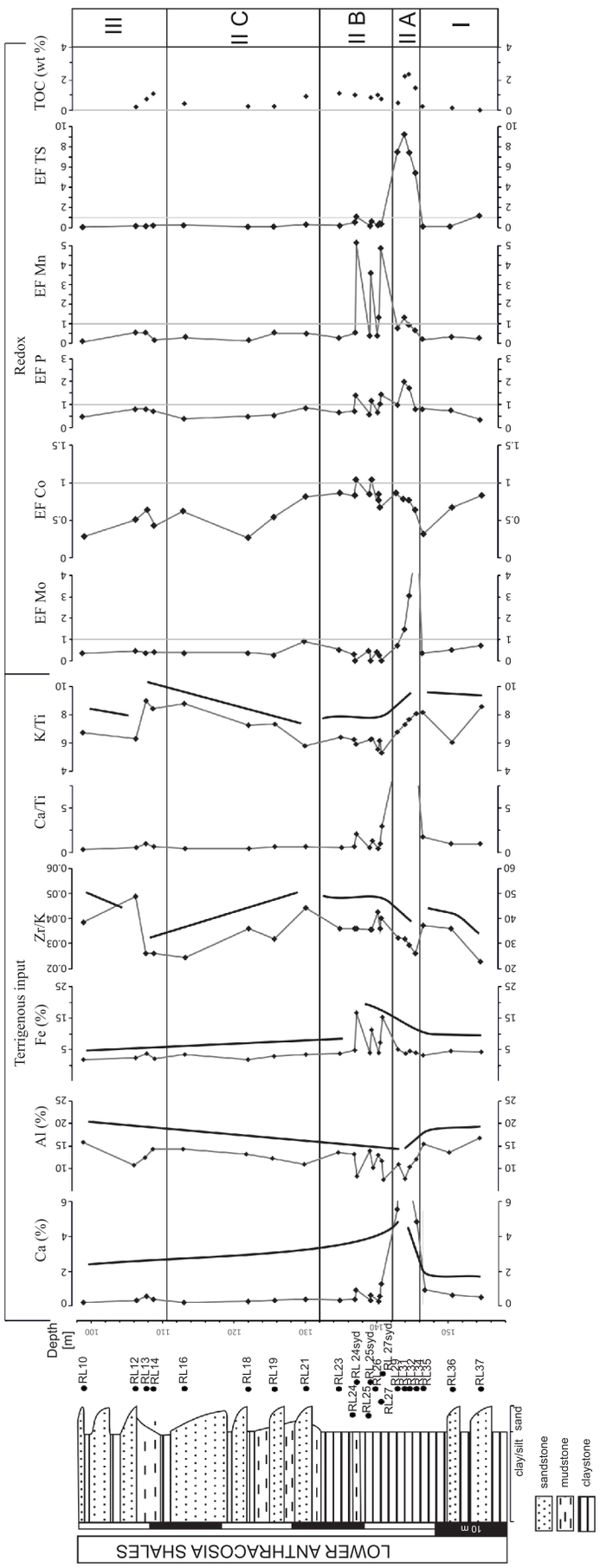

Fig. 7. Stratigraphic distribution of proxies related to the chemistry of the lake, such as the detrital input and redox regime

step. Thus, Mo accumulation in the calcareous rocks of interval IIA indicates the occurrence of relatively reductive (anoxic) conditions. The low rate of sedimentation could have favoured the incorporation of Mo into the sediment.

The distribution of Mo is opposite to and independent that of Fe and Mn in intervals IIB and IIC. A slightly higher Mo content occurs in the samples that are poor in Fe-Mn (Fig. 7). In contrast, the Co distribution shows a little enrichment in the sideritic samples. Cobalt is fluvially delivered as the dissolved cation, or complexed with soil organic acids. In anoxic conditions, Co forms the insoluble sulphide CoS, which can be incorporated as a minor constituent in Fe-sulphides (Huerta-Diaz and Morse, 1992).

Mo and Co are strongly associated with the sulphide fraction, but oxyanion-forming elements (e.g., Mo) are trapped in syngenetic pyrite, whereas diagenetic pyrite contains relatively more heavy metals (e.g., Co) (Berner et al., 2013). Thus, Co accumulation in the sideritic layers of interval IIB is related to sediment anoxia and diagenetic pyritization.

A suboxic or "manganous" redox regime is also indicated by the Mn concentrations (Canfield and Thamdrup, 2009; Wirth et al., 2013), where Mn enrichment might be taken as an indicator of occasional water-column ventilation during anoxic conditions (Calvert and Pedersen, 1996). The Mn/Fe ratio has been widely employed as a proxy for past lake oxygenation (Naeher et al., 2013; Makri et al., 2021), with the assumption that low Mn/Fe ratios may indicate reducing conditions, whereas high Mn/Fe ratios are likely related to increased O_2 concentrations (Mackereth, 1966; Wersin et al., 1991). However, Fe and Mn content and the elemental ratio were controlled by many factors other than redox conditions during times of high detrital input, and/or higher supply of dissolved organic carbon and diagenetic processes (Makri et al., 2021). Intervals IIA and IIB reveal the co-occurrence of Fe-Mn-P and TOC, as well as TS that can be mainly related to anoxia and diagenetic processes of Mn uptake in the sediments as carbonate, phosphate and/or sulphide minerals. Fe and Mn carbonates are readily formed under reducing conditions (Håkanson and Jansson, 1983). Phosphate mineral such as vivianite or phosphoferrite can precipitate in the sediment from reducing pore-water (Nriagu and Dell, 1974; Håkanson and Jansson, 1983). Their presence in all samples suggests that the rocks were saturated with reducing solutions.

DISCUSSION

Our mineralogical-geochemical study of the Rybnica Leśna PIG 1 borehole core section shows significant variations in terrigenous supply to the sedimentary basin throughout the Late Carboniferous/Early Permian. The variations expressed by mineralogical-geochemical indices and lithology were primarily controlled by climatic chan-

ges. The Pennsylvanian witnessed a major glaciation onset probably related to the final assembly of Pangea as a result of the Variscan orogeny (e.g., Crowley and Baum, 1992; Fielding et al., 2008). Global sea level fluctuation could have caused humid-arid changes on land; therefore, sedimentation in the continental basins was probably controlled by a complex interplay of climatic and tectonic forcing (Stollhofen et al., 1999; Falcon-Lang, 2004; Izart et al., 2005).

The Rybnica Leśna PIG 1 section records the lake evolution influenced by tectonics and a humid climate phase. The Intra-Sudetic Basin was a place where wet periods occurred repeatedly, accompanied by the accumulation of black claystones or coal seams (Wołkowicz, 1988; Mastalerz, 1990; Mastalerz and Nehyba, 1997; Bossowski and Ihnatowicz, 2006). The succession contains a few volcanoclastic layers, suggesting the enhanced volcanic activity of the Sudetic area related to the Varicides development (Awdankiewicz et al., 2003; Awdankiewicz, 2022).

An analogous combination of climate and tectonics has been discussed regarding the lacustrine system of the Saar-Nahe and Bohemian basins (Stollhofen et al., 1999; Lojka et al., 2009). Periodic humidification at the Kasimovian-Gzhelian (Stephanian) has been correlated to the Gondwana deglaciation cycle, with a wet interval in Central Europe (Roscher and Schneider, 2006).

In the section studied, the calcareous black claystones record the maximum depth of the Anthracosia Basin, which would have developed stepwise and later became supplied by terrestrial material, as proposed by Mastalerz and Nehyba (1997); therefore, interval I represents the beginning of transgression, interval IIA refers to the lake highstand followed by a gradual lake-level fall accompanied by intense input of terrestrial material (IIB), regression (IIC), and finally, lake termination (III).

The initial stage of the lake was probably related to rising humidity, consequently accompanied by fluvial transport. Interval I is rich in siliciclastic material, whose occurrence in tropical lacustrine sediments can mirror huge floods (Giresse et al., 1991). Generally, wet conditions favoured progressive weathering that triggered a stepwise increase in the supply of weathering products (e.g., Fe-Mn compounds) to the lake (Irion et al., 2006; Lojka et al., 2009) throughout intervals I and IIA. The black claystones of interval IIA represent the deepest facies of the Anthracosia Basin with limited detrital input and dominant calcite sedimentation. For that reason, Zr accumulation is low. The K/Ti ratio tends to be lower, indicating chemical weathering. During the highstand of the lake, well-defined lamination was scarcely formed. In comparison with modern analogues of a tropical lake (Giresse et al., 1991), organic-rich poorly laminated claystone is a deposit of a generally stable environment (low seasonality). A humid climate could have resulted in effective nutrient supply, and maximum productivity, linked with permanent water column stratification producing lake-floor anoxia. The anoxic (sulphidic) condition of the black claystones of interval IIA have been demonstrated by the enrichment in Mo, TS and small, abundant framboids. This interpretation is consistent with the results of analysis of organic matter from the Anthracosia Shales. The maceral composition, miospore assemblages and palynofacies occurring in the fine-grained lithology enriched in OM were classified as bituminous associations typical of a deep-water zone near the centre of the LAS. It records high bio-productivity of the surface water and reducing depositional conditions (Nowak et al., 2022).

The highstand was followed by a gradual lake-level fall recorded in interval IIB. Well-pronounced lamination with silt laminae and siderite indicates rhythmic seasonality accompanied by increased sediment supply. The lamination of the LAS related to seasonal changes was also postulated based on organic petrology (Nowak et al., 2022). Detritus delivered to the lake had been previously affected by intense chemical decay in humid and warm conditions, shown by the high Fe-Mn content and low K/Ti ratio in the rocks of interval IIB. The sideritic layers may record permanent anoxia in the sediments and early diagenetic processes, and seasonally changing oxygenation of bottom water as suggested by Co concentrations, fluctuations of the Mn/Fe ratio and the larger pyrite framboids. The lack of fossils together with undisturbed lamination suggest that the environment was not hospitable to living organisms.

The increased thickness of silt laminae in interval IIC indicates seasonality, perhaps related to monsoonal circulation, and a stepwise regression. The drop in Fe-Mn content and increasing K/Ti ratio suggest decreasing chemical weathering due to aridification. During the lake stage represented by interval IIC, the lake-floor conditions turned oxic with the disappearance of pyrite.

Frequent interruptions of turbiditic sandy laminae in interval III suggest the terminal stage of lake infill, characterized by more pronounced sediment flux. A decline in kaolinite content in the upper part of the section (Wójcik-Tabol et al., 2021) may indicate less intense chemical weathering in the drainage basin at the time when interval III was formed. However, the low K/Ti ratio an d high Zr may also record a volcanoclastic contribution. Organic matter of this interval represents a humic association deposited in a coastal zone. Terrigenous organic matter was usually not transported over long distances. Some microscopically visible organic fragments (inertinite) indicate a high-temperature origin, most likely caused by forest fires (Nowak et al., 2022), which may indicate dry conditions during the Anthracosia lake's existence.

Evaporation was not an exclusive reason for the Anthracosia Basin's termination. The intensity of precipitation significantly influenced the lake's development, stimulating productivity, stratification and sediment supply, while the system was also affected by the tectonic evolution of the drainage basin and volcanic activity.

CONCLUSIONS

The Anthracosia Basin deposits represent a valuable environmental record of the Pennsylvanian and the Early Permian within the Variscan orogenic belt in eastern equatorial Pangaea. The Rybnica Leśna PIG 1 section demonstrates lacustrine system evolution within the Intra-Sudetic Basin that may have been controlled by the interplay of climatic and tectonic forcing.

The climate was humid during the start of the Anthracosia Basin sedimentation. The black claystones of interval IIA are facies of an open lake formed under an almost non-seasonal climate, linked with permanent water column stratification and anoxia. The highstand gradually shifted into a seasonally humid climate and intense chemical weathering. Interval IIB with sideritic layers may record permanent anoxia in the sediments and early diagenetic processes, and seasonally changing oxygena-

tion of the bottom water. The later lake regression (interval IIC) may be related to climate aridification, followed by interval III of the terminal infill of the basin. The climate interval represented in this work corresponds with a Late Pennsylvanian wet phase, likely linked to a southern Gondwana interglacial episode.

Acknowledgements. This research has been supported by a grant from the Faculty of Geography and Geology under the Strategic Programme Excellence Initiative at the Jagiellonian University, Kraków.

REFERENCES

Algeo, T.J., Maynard, J.B., 2004. Trace-element behavior and redox facies in core shales of Upper Pennsylvanian Kansas-type cyclothems. Chemical Geology, **206**: 289–318. https://doi.org/10.1016/j.chemgeo.2003.12.009

Arnaud, F., Révillon, S., Debret, M., Revel, M., Chapron, E., Jacob, J., Giguet-Covex, C., Poulenard, J., Magny, M., 2012. Lake Bourget regional erosion patterns reconstruction reveals Holocene NW European Alps soil evolution and paleohydrology. Quaternary Science Reviews, **51**: 81–92. https://doi.org/10.1016/j.quascirev.2012.07.025

Awdankiewicz, M., 1999. Volcanism in a late Variscan intramontane trough: Carboniferous and Permian volcanic centres of the Intra-Sudetic Basin, SW Poland. Geologia Sudetica, **32**: 13–47.

Awdankiewicz, M., 2022. Polyphase Permo-Carboniferous magmatism adjacent to the Intra-Sudetic Fault: constraints from U-Pb SHRIMP zircon study of felsic subvolcanic intrusions in the Intra-Sudetic Basin, SW Poland. International Journal of Earth Sciences, **111**: 2199–2224. https://doi.org/10.1007/s00531-022-02232-y

Awdankiewicz, M., Kurowski, L., Mastalerz, K., Raczyński, P., 2003. The Intra-Sudetic Basin – a record of sedimentary and volcanic processes in late – to post-orogenic tectonic setting. GeoLines, **16**: 165–183.

Bahrig, B., 1989. Stable isotope composition of siderite as an indicator of the paleoenvironmental history of oil shale lakes. Palaeogeography, Palaeoclimatology, Paleoecology, **70**: 139–151. https://doi.org/10.1016/0031-0182(89)90085-0

Bassetti, M.A., Berné, S., Sicre, M.A., Dennielou, B., Alonso, Y., Buscail, R., Jalali, B., Hebert, B., Menniti, C., 2016. Holocene hydrological changes in the Rhône River (NW Mediterranean) as recorded in the marine mud belt. Climate of the Past, **12**: 1539–1553. https://doi.org/10.5194/cp-12-1539-2016

Berg, W.F.M., 1938. Crystal growth from solutions. Proceedings of the Royal Society of London. Series A-Mathematical and Physical Sciences, **164**: 79–95.

Berner, Z.A., Puchelt, H., Noeltner, T., Kramar, U.T.Z., 2013. Pyrite geochemistry in the Toarcian Posidonia Shale of south-west Germany: evidence for contrasting trace-element patterns of diagenetic and syngenetic pyrites. Sedimentology, **60**: 548–573. https://doi.org/10.1111/j.1365-3091.2012.01350.x

Bond, D.P., Wignall, P.B., 2010. Pyrite framboid study of marine Permian–Triassic boundary sections: a complex anoxic event and its relationship to contemporaneous mass extinction. GSA Bulletin, **122**: 1265–1279. https://doi.org/10.1130/B3004

Bossowski, A., Ihnatowicz, A., 1994. Palaeogeography of the uppermost Carboniferous and lowermost Permian deposits in the NE part of the Intra-Sudetic Depression. Geological Quarterly, **38** (4): 709–726.

Bossowski, A., Ihnatowicz, A., 2006. Geological Atlas of the Lower Silesian Coal Basin. Państwowy Instytut Geologiczny, Warszawa.

Calvert, S.E., Pedersen, T.F., 1993. Geochemistry of recent oxic and anoxic marine sediments: implications for the geological record. Marine Geology, **113**: 67–88. https://doi.org/10.1016/0025-3227(93)90150-T

Calvert, S.E., Pedersen, T.F., 1996. Sedimentary geochemistry of manganese; implications for the environment of formation of manganiferous black shales. Economic Geology, **91**: 36–47. https://doi.org/10.2113/gsecongeo.91.1.36

Canfield, D.E., Thamdrup, B.O., 2009. Towards a consistent classification scheme for geochemical environments, or, why we wish the term 'suboxic' would go away. Geobiology, **7**: 385–392. https://doi.org/10.1111/j.1472-4669.2009.00214.x

Clift, P.D., Wan, S., Blusztajn, J., 2014. Reconstructing chemical weathering, physical erosion and monsoon intensity since 25 Ma in the northern South China Sea: a review of competing proxies. Earth-Science Reviews, **130**: 86–102. https://doi.org/10.1016/j.earscirev.2014.01.002

Crowley, T.J., Baum, S.K., 1992. Modeling late Paleozoic glaciation. Geology, **20**: 507–510. https://doi.org/10.1130/0091-7613(1992)020<0507:MLPG>2.3.CO;2

Dahl, T.W., Hammarlund, E.U., Anbar, A.D., Bond, D.P., Gill, B.C., Gordon, G.W., Knoll, A.H., Nielsen, A.T., Schovsbo, N.H., Canfield, D.E., 2010. Devonian rise in atmospheric oxygen correlated to the radiations of terrestrial plants and large predatory fish. Proceedings of the National Academy of Sciences, **107**: 17911–17915. https://doi.org/10.1073/pnas.1011287107

Don, J., 1961. The Permo-Carboniferous of the Nowa Ruda region (in Polish with English summary). Zeszyty Naukowe Uniwersytetu Wrocławskiego, Nauka o Ziemi, **3**: 3–49.

Döbelin, N., Kleeberg, R., 2015. Profex: a graphical user interface for the Rietveld refinement program BGMN. Journal of Applied Crystallography, **48**: 1573–1580. https://doi.org/10.1107/S1600576715014685

Dypvik, H., Harris, N.B., 2001. Geochemical facies analysis of fine-grained siliciclastics using Th/U, Zr/Rb and (Zr+ Rb)/Sr ratios. Chemical Geology, **181**: 131–146. https://doi.org/10.1016/S0009-2541(01)00278-9

Dziedzic, K., 1959. Comparison on Rotliegendes sediments in the region of Nowa Ruda (Middle Sudetes) (in Polish with English summary). Geological Quarterly, **3** (4): 831–846.

Dziedzic, K., 1961. Lower Permian in the Intrasudetic Basin. Studia Geologica Polonica, **6**: 1–124.

Dziedzic, K., 1971. Sedimantation and palaeogeography of the Upper Carboniferous deposits in the Intrasudetic Depression (in Polish with English summary). Geologia Sudetica, **5**: 7–75.

Dziedzic, K., Teisseyre, A.K., 1990. The Hercynian molasse and younger deposits in the Intra-Sudetic Depression, SW Poland. Neues Jahrbuch für Geologie und Paläontologie Abhandlungen, **179**: 285–305.

Eagar, R.M.C., 1987. The shape of the Upper Carboniferous non-marine bivalve *Anthraconaia* in relation to the organic carbon content of the host sediment. Earth and Environmental Science Transactions of the Royal Society of Edinburgh, **78**: 177–195. https://doi.org/10.1017/S0263593300011093

Falcon-Lang, H.J., 2004. Pennsylvanian tropical rain forests responded to glacial-interglacial rhythms. Geology, **32**: 689–692. https://doi.org/10.1130/G20523.1

Fielding, C.R., Frank, T.D., Isbell, J.L., 2008. The late Paleozoic ice age – a review of current understanding and synthesis of global climate patterns. GSA, Special Paper, **441**: 343–354. https://doi.org/10.1130/2008.2441(24)

Gastaldo, R.A., DiMichele, W.A., Pfefferkorn, H.W., 1996. Out of the icehouse into the greenhouse: a late Paleozoic analogue for modern global vegetational change. GSA Today, **6**: 1–7.

Giresse, P., Maley, J., Kelts, K., 1991. Sedimentation and palaeoenvironment in crater lake Barombi Mbo, Cameroon, during the last 25,000 years. Sedimentary Geology, **71**: 151–175. https://doi.org/10.1016/0037-0738(91)90099-Y

Górecka, T., 1981. Results of palynological studies of the Youngest Carboniferous of the Lower Silesia (in Polish with English summary). Prace Naukowe Instytutu Górnictwa Politechniki Wrocławskiej, **40**: 1–58.

Górecka-Nowak, A., 1989. Late Carboniferous spore-pollen assemblages of the Unisław IG-1 bore hole (in Polish with English summary). Prace Naukowe Instytutu Górnictwa Politechniki Wrocławskiej, 52, Studia i Materiały, **19**: 51–57.

Górecka-Nowak, A., 1995. Palynostratigraphy of the Westphalian deposits of the nort-western part of the Intrasudetic Basin (in Polish with English summary). Acta Universitatis Wratislaviensis, Prace Geologiczno-Mineralogiczne, **40**: 1–156.

Górecka-Nowak, A., 2008. Palynostratigraphy of the uppermost Carboniferous and lowermost Permian sediments in the Sudetes (SW Poland). 12th International Palynological Congress. Terra Nostra, **2**: 97.

Górecka-Nowak, A., Nowak, G.J., 2008. Charakterystyka petrologiczna i palinologiczna materii organicznej czarnych łupków Sudetów (in Polish). First Polish Geological Congres (ed. G. Haczewski): 32, Kraków, Abstracts.

Grabowski, J., Chmielewski, A., Ploch, I., Rogov, M., Smoleń, J., Wójcik-Tabol, P., Leszczyński, K., Maj-Szeliga, K., 2021a. Palaeoclimatic changes and inter-regional correlations in the Jurassic/Cretaceous boundary interval of the Polish Basin: portable XRF and magnetic susceptibility study. Newsletters on Stratigraphy, **54**: 123–158. https://doi.org/10.1127/nos/2020/0600

Grabowski, J., Stoykova, K., Wierzbowski, H., Wójcik-Tabol, P., 2021b. Upper Berriasian chemostratigraphy, clay minerals and calcareous nannofossils of the Barlya section (Western Balkan, Bulgaria): implications for palaeoclimate and productivity changes, and stratigraphic correlations across the Alpine Tethys. Palaeogeography, Palaeoclimatology, Palaeoecology, **567**: 110252. https://doi.org/10.1016/j.palaeo.2021.110252

Håkanson, L., Jansson, M., 1983. Principles of Lake Sedimentology. Springer-Verlag, Berlin.

Helz, G.R., Miller, C.V., Charnock, J.M., Mosselmans, J.F.W., Pattrick, R.A.D., Garner, C.D., Vaughan, D.J., 1996. Mechanism of molybdenum removal from the sea and its concentration in black shales: EXAFS evidence. Geochimica et Cosmochimica Acta, **60**: 3631–3642. https://doi.org/10.1016/0016-7037(96)00195-0

Huerta-Diaz, M.A., Morse, J.W., 1992. Pyritization of trace metals in anoxic marine sediments. Geochimica et Cosmochimica Acta, **56**: 2681–2702. https://doi.org/10.1016/0016-7037(92)90353-K

Irion, G., Bush, M.B., De Mello, J.N., Stüben, D., Neumann, T., Müller, G., Junk, J.W., 2006. A multiproxy palaeoecological record of Holocene lake sediments from the Rio Tapajós, eastern Amazonia. Palaeogeography, Palaeoclimatology, Palaeoecology, **240**: 523–535. https://doi.org/10.1016/j.palaeo.2006.03.005

Izart, A., Palain, C., Malartre, F., Fleck, S., Michels, R., 2005. Paleoenvironments, paleoclimates and sequences of Westphalian deposits of Lorraine coal basin (Upper Carboniferous, NE France). Bulletin de la Société Géologique de France, **176**: 301–315. https://doi.org/10.2113/176.3.301

Jerzykiewicz, J., 1987. Latest Carboniferous (Stephanian) and Early Permian (Autunian) palynological assemblages from the Intra-sudetic Basin, southwestern Poland. Palynology, **11**: 117–131. https://doi.org/10.1080/01916122.1987.9989324

Kowalski, A., Furca, M., 2023. Development of a non-perennial to ephemeral fluvial system in continental fault-bounded basin–an example from the early Permian Krajanów Formation of the Intra-Sudetic Basin (NE Bohemian Massif). Geological Quarterly, **67**: 31. http://dx.doi.org/10.7306/gq.1701

Li, Y.H., Schoonmaker, J.E., 2003. Chemical composition and mineralogy of marine sediments. Treatise on Geochemistry, **7**: 1–35. https://10.1016/B0-08-043751-6/07088-2

Liu, H., Qiu, Z., Zou, C., Fu, J., Zhang, W., Tao, H., Chen, Z.Q., 2021. Environmental changes in the Middle Triassic lacustrine basin (Ordos, North China): implication for biotic recovery of freshwater ecosystem following the Permian-Triassic mass extinction. Global and Planetary Change, **204**: 103559. https://doi.org/10.1016/j.gloplacha.2021.103559

Lojka, R., Drábková, J., Zajíc, J., Sýkorová, I., Franců, J., Bláhová, A., Grygar, T., 2009. Climate variability in the Stephanian B based on environmental record of the Mšec Lake deposits (Kladno–Rakovník Basin, Czech Republic). Palaeogeography, Palaeoclimatology, Palaeoecology, **280**: 78–93. https://doi.org/10.1016/j.palaeo.2009.06.001

Lojka, R., Sýkorová, I.V.A.N.A., Laurin, J.I.Ř.Í., Matysova, P., Matys Grygar, T., 2010. Lacustrine couplet-lamination: evidence for Late Pennsylvanian seasonality in central equatorial Pangaea (Stephanian B, Mšec Member, Central and Western Bohemian basins). Bulletin of Geosciences, **85**: 709–734. https://doi.org/10.314/bull.geosci.1210

Lorenc, S., 1993. Distribution, lithology and approximate geochemical features of the Sudetes black shales (in Polish with English summary). Prace Geologiczno-Mineralogiczne, **33**: 179–208.

Mackereth, F.J., 1966. Some chemical observations on post-glacial lake sediments. Philosophical Transactions of the Royal Society of London. Series B, Biological Sciences, **250**: 165–213. https://doi.org/10.1098/rstb.1966.0001

Makri, S., Wienhues, G., Bigalke, M., Gilli, A., Rey, F., Tinner, W., Vogel, H., Grosjean, M., 2021. Variations of sedimentary Fe and Mn fractions under changing lake mixing regimes, oxygenation and land surface processes during Late-glacial and Holocene times. Science of the Total Environment, **755**: 143418. https://doi.org/10.1016/j.scitotenv.2020.143418

Martínek, K., Blecha, M., Daněk, V., Franců, J., Hladíková, J., Johnová, R., Uličný, D., 2006. Record of palaeoenvironmental changes in a Lower Permian organic-rich lacustrine succession: integrated sedimentological and geochemical study of the Rudník member, Krkonoše Piedmont Basin, Czech Republic. Palaeogeography, Palaeoclimatology, Palaeoecology, **230**: 85–128. https://doi.org/10.1016/j.palaeo.2005.07.009

Mastalerz, K., 1990. Lacustrine successions in fault bounded basins: 1. Upper Anthracosia Shale (Lower Permian) of the North Sudetic Basin, SW Poland. Annales Societatis Geologorum Poloniae, **60**: 75–106.

Mastalerz, K., Nehyba S., 1997. Comparison of Rotliegende lacustrine depositional sequences from the Intrasudetic, Northsudetic and Boskovice basins (Central Europe). Geologia Sudetica**, 30:** 21–58.

Mazur, S., Aleksandrowski, P., Kryza, R., Oberc-Dziedzic, T., 2006. The Variscan orogen in Poland. Geological Quarterly, **50** (1): 89–118.

Miecznik, J.B., 1989. The Upper Silesian and Lower Autunian from NE limb of the Intra-Sudetic Depression (in Polish with English summary). Biuletyn Państwowego Instytutu Geologicznego, **363**: 5–40.

Montañez, I.P., Poulsen, C.J., 2013. The Late Paleozoic ice age: an evolving paradigm. Annual Review of Earth and Planetary Sciences, **41**: 629–656. https://doi.org/10.1146/annurev.earth.031208.10011

Naeher, S., Gilli, A., North, R.P., Hamann, Y., Schubert, C.J., 2013. Tracing bottom water oxygenation with sedimentary Mn/Fe ratios in Lake Zurich, Switzerland. Chemical Geology, **352**: 125–133. https://doi.org/10.1016/j.chemgeo.2013.06.006

Nemec, W., Porębski, S., Teisseyre, A.K., 1982. Explanatory notes to the lithotectonic molasse profile of the Intra-Sudetic Basin, Polish Part. Veröffentlichungen des Zentralinstituts für Physik der Erde, Akademie der Wissenschaften der DDR, **66**: 267–278.

Nowak, G.J., 1998. Microscopic identification and classification of organic matter of the Upper Carboniferous Anthracosia Shales, Intra-Sudetic Depression, southwestern Poland. Geological Quarterly, **42** (1): 41–58.

Nowak, G.J., 2003. Petrology of organic matter dispersed in Late Palaeozoic sedimentary rocks of south western Poland (in Polish with English summary). Cuprum, **4**: 1–209.

Nowak, G.J., 2007. Comparative studies of organic matter petrography of the late palaeozoic black shales from Southwestern Poland. International Journal of Coal Geology, **71**: 568–585.? https://doi.org/10.1016/j.coal.2007.01.004

Nowak, G.J., Górecka-Nowak, A., Karcz, P., 2022. Petrographic, palynological and geochemical recognition of dispersed organic matter in the black Anthracosia Shales (Sudetes, south-west Poland). Geological Quarterly, **66** (4): 66–36. http://doi.org/10.7306/gq.1668

Nriagu, J.O., Dell, C.I., 1974. Diagenetic formation of iron phosphates in recent lake sediments. American Mineralogist, **59**: 934–946.

Rachold, V., Brumsack, H.J., 2001. Inorganic geochemistry of Albian sediments from the Lower Saxony Basin NW Germany: palaeoenvironmental constraints and orbital cycles. Palaeogeography, Palaeoclimatology, Palaeoecology, **174**: 121–143. https://doi.org/10.1016/S0031-0182(01)00290-5

Rickard, D., 2021. Framboids. Oxford University Press.

Roscher, M., Schneider, J.W., 2006. Permo-Carboniferous climate: Early Pennsylvanian to Late Permian climate development of central Europe in a regional and global context. Geological Society, London, Special Publications, **265**: 95–136. https://doi.org/10.1144/GSL.SP.2006.265.01.05

Rust, G.W., 1935. Colloidal primary copper ores at Cornwall Mines, southeastern Missouri. The Journal of Geology, **43**: 398–426. https://doi.org/10.1086/624318

Sawłowicz, Z., 1993. Pyrite framboids and their development: a new conceptual mechanism. Geologische Rundschau, **82**: 148–156. https://doi.org/I: 10.1007/BF00563277

Sawłowicz, Z., 2000. Framboids: from their origin to application. Wydawnictwo Oddziału Polskiej Akademii Nauk, Warszawa.

Stollhofen, H., Frommherz, B., Stanistreet, I.G., 1999. Volcanic rocks as discriminants in evaluating tectonic versus climatic control on depositional sequences, Permo-Carboniferous continental Saar-Nahe Basin. Journal of the Geological Society, **156**: 801–808. https://doi.org/10.1144/gsjgs.156.4.0801

Taylor, S.R., McLennan, S.M., 1985. The Continental Crust: its Composition and Evolution. Blackwell Publication, United States.

Tribovillard, N., Algeo, T.J., Lyons, T., Riboulleau, A., 2006. Trace metals as paleoredox and paleoproductivity proxies: an update. Chemical Geology, **232**: 12–32. https://doi.org/10.1016/j.chemgeo.2006.02.012

Trzepierczyńska, A., 1994. Microfloristic studies of the Ścinawka Dolna IG-1 borehole. In: Palaeogeography of the Upper Carboniferous and Lower Autunian deposits in the Nowa Ruda region. (ed. A. Bossowski). Polish Geological Institute, NAG: 728/94.

Uffmann, A.K., Littke, R., Rippen, D., 2012. Mineralogy and geochemistry of Mississippian and Lower Pennsylvanian black shales at the northern margin of the Variscan Mountain Belt (Germany and Belgium). International Journal of Coal Geology, **103**: 92–108. https://doi.org/10.1016/j.coal.2012.08.001

Wei, H., Jiang, X., 2019. Early Cretaceous ferruginous and its control on the lacustrine organic matter accumulation: constrained by multiple proxies from the Bayingebi Formation in the Bayingebi Basin, inner Mongolia, NW China. Journal of Petroleum Science and Engineering, **178**: 162–179. https://doi.org/10.1016/j.petrol.2019.03.037

Wersin, P., Höhener, P., Giovanoli, R., Stumm, W., 1991. Early diagenetic influences on iron transformations in a freshwater lake sediment. Chemical Geology, **90**: 233–252. https://doi.org/10.1016/0009-2541(91)90102-W

Wilkin, R.T., Barnes, H.L., Brantley, S.L., 1996. The size distribution of framboidal pyrite in modern sediments: an indicator of redox conditions. Geochimica et Cosmochimica Acta, **60**: 3897–3912. https://doi.org/10.1016/0016-7037(96)00209-8

Wirth, S.B., Gilli, A., Niemann, H., Dahl, T.W., Ravasi, D., Sax, N., Hamann, Y., Peduzzi, R., Peduzzi, S., Tonolla, M., Lehmann, M.F., Anselmetti, F.S., 2013. Combining sedimentological, trace metal (Mn, Mo) and molecular evidence for reconstructing past water-column redox conditions: the example of meromictic Lake Cadagno (Swiss Alps). Geochimica et Cosmochimica Acta, **120**: 220–238. https://doi.org/10.1016/j.gca.2013.06.017

Wołkowicz, S., 1988. On the sedimentation of the Lower Permian Walchia shales from Ratno Dolne (Intra-Sudetic Depression) (in Polish with English summary). Przegląd Geologiczny, **36**: 214–218.

Wójcik-Tabol, P., Dąbek, J., Nowak, G.J., 2021. Preliminary mineralogical characteristics of the Anthracosia Shales from the Intra-Sudetic Synclinorium (in Polish with English summary). Przegląd Geologiczny, **69**: 389–392. https://doi.org/10.7306/2021.23

Yuan, W., Liu, G., Stebbins, A., Xu, L., Niu, X., Luo, W., Li, C., 2017. Reconstruction of redox conditions during deposition of organic-rich shales of the Upper Triassic Yanchang Formation, Ordos Basin, China. Palaeogeography, Palaeoclimatology, Palaeoecology, **486**: 158–170. https://doi.org/10.1016/j.palaeo.2016.12.020